Hindawi Publishing Corporation
Mathematical Problems in Engineering
Volume 2016, Article ID 1468629, 16 pages
http://dx.doi.org/10.1155/2016/1468629

Research Article

Impact Pseudostatic Load Equivalent Model and the Maximum Internal Force Solution for Underground Structure of Tunnel Lining

Xuan Guo[1] and Xiao Xin Zhang[2]

[1]*School of Civil Engineering, Beijing Jiaotong University, Beijing 100044, China*
[2]*China Construction Engineering Design Group Corporation Limited, Beijing 100037, China*

Correspondence should be addressed to Xuan Guo; xguo@bjtu.edu.cn

Received 13 May 2016; Accepted 16 October 2016

Academic Editor: Manuel Pastor

The theoretical formula of the maximum internal forces for circular tunnel lining structure under impact loads of the underground is deduced in this paper. The internal force calculation formula under different equivalent forms of impact pseudostatic loads is obtained. Furthermore, by comparing the theoretical solution with the measured data of the top blasting model test of circular formula under different equivalent forms of impact pseudostatic loads are obtained. Furthermore, by comparing the theoretical solution with the measured data of the top blasting model test of circular tunnel, it is found that the proposed theoretical results accord with the experimental values well. The corresponding equivalent impact pseudostatic triangular load is the most realistic pattern of all test equivalent forms. The equivalent impact pseudostatic load model and maximum solution of the internal force for tunnel lining structure are partially verified.

1. Introduction

In recent years, the nuclear leakage events have sparked a new national self-examination. The safety and stability problems of the underground structure caused by the impact or blasting load must be paid special attention to. The blasting demolition at the top of underground, chemical explosion devised by terrorism, gas pressure extrusion, and release of shallow layer containing gas and so forth will result in instant huge impact load on the structure of tunnel lining. The structure crack or damage of the tunnel under the impact load will lead directly to the serious nuclear leakage events, with Japan's Fukushima nuclear power plant explosion causing the serious nuclear leakage from 2011. The former Soviet Union Chernobyl nuclear power plants exploded at 1:23 in the morning of April 26, 1986, with more than 8 tons of highly radioactive materials mixed with graphite fragments and nuclear fuel burning debris spewing out. The radiation pollution caused by the nuclear leakage accident is equivalent to 100 times of the radioactive pollution caused by the atomic bomb explosion in Hiroshima, Japan. Even 20 days after the accident, the temperature of the center of the nuclear reactor is still as high as 270 degrees Celsius. It caused 10 times the number of cancer deaths caused by the accident in the United Nations official estimates, with a global total of 2 billion people affected by the Chernobyl accident; 270 thousand people suffer from cancer, which killed more than 93 thousand people. Experts estimate that eliminating the effects of this catastrophe will take at least 800 years.

The underground structure of tunnel lining locates in the enclosure space; the security problem and the precise evaluation of the dynamic response to the blasting or impact loading becomes an important engineering issue and there is a need to give mathematical model and solution of internal force [1–6].

First, determining the strength and internal force of structure response under the blast loading is the key factor to solve the dynamic response problem for tunnel lining. By now, the researches of stability of the structure for tunnel lining under impact load are more concentrated in blasting

load or gas outburst. Generalized impact action blocks and changes the motion of a moving object. The difference between impact load and impact pseudostatic load is the energy form related to the instantaneous time effect or not. Generally, the quantity of explosive and detonation pressure of explosive shock can be determined according to the energy release and the size of the gas pressure to determine the impact of the air pressure. Blasting seismic wave attenuation can be equivalent to the dynamic load effect of gas outburst on tunnel lining structure. Currently, the theoretical study of the tunnel lining and the internal force response under impact load is relatively little. This paper introduces the free deformation method as the theoretical basis. Derivation of impact load equivalent pseudostatic model is given. Load pattern on the circular tunnel lining under the instantaneous maximum internal force calculation formula is compared and analyzed. By comparing the theoretical analysis to the test data and the numerical simulation results, it intends to get the internal force response of the failure mechanism and the optimal load pattern and the theoretical results can be preliminarily verified by the back analysis [1].

2. The Internal Force Formula of the Circular Tunnel Lining under the Blasting Loading

Considering significantly attenuated effect of cover layer to the impact load and wave, it is supposed that impact loaded on structure of tunnel lining is equal to the earth surface. The additional stresses during elastic wave propagation are ignored. To simulate the stress and deformation of tunneling lining under impact or blasting dynamic load, engineers commonly adopt the simple and safe simplified method, which means the impact pseudostatic load multiplied by a dynamic load factor to estimate the maximum impact load. The core idea of the proposed method is first to find out the maximum equivalent impact pseudostatic stress mode under the impact or blasting load.

The theory formula of the equivalent model for impact load on circular tunnel lining is derived based on using the free deformation method, which is the classical theory method for underground structure [7].

2.1. The Equivalent Impact Load Model. The equivalent impact load model should be given and the equivalent form caused by blasting seismic wave loads on tunnel lining structure should be determined. Left-side blasting load coefficient of dynamic stress distribution for surrounding rock is given by Figure 1. Figure 1(a) gives the mechanical model of left-side blasting load on the circular underground structure; the radial movement of surrounding rock stress concentration factor is given as in Figure 1(b). Upper blasting load coefficient of dynamic stress distribution of surrounding rock is shown in Figure 2. Figure 2(a) gives the mechanical model of the upper-side blasting load on the circular underground structure; the force model of the tunnel lining structure and the surrounding rock of the dynamic stress concentration factor distribution map is given as in Figure 2(b). Figure 1 can give the maximum acceleration stress distribution map of the left-side blasting load in surrounding rock for lining. Figure 2

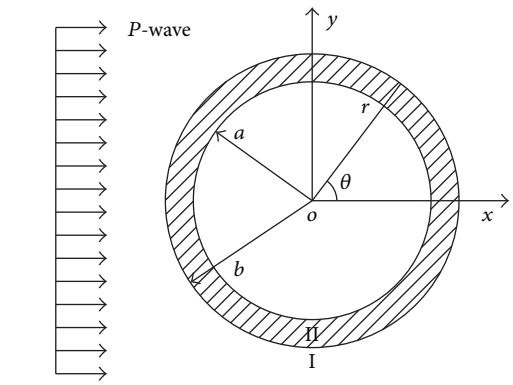

(a) Mechanical model

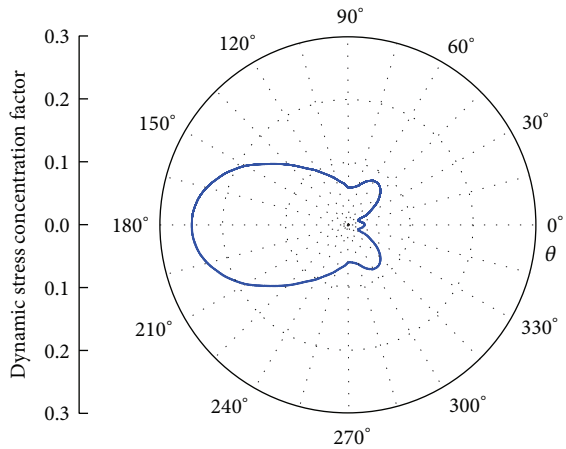

(b) Radial movement of surrounding rock stress concentration factor

Figure 1: Left-side blasting load coefficient of dynamic stress distribution for surrounding rock [8].

can give the maximum acceleration stress distribution map of the upper-side blasting load surrounding rock for lining. From Figures 1 and 2, it is shown that the blasting response of the circular lining is according to the following rules: the maximum point of impact load generally is the maximum stress response point, mostly on angle of 0 degrees near the load; the smaller load is distributed on both sides of the lining; the maximum stress zone is concentrated in the range of ±15 degrees around both sides of the impact load; on the far side from the impact load, the stress on both ends of the lining is obviously higher than that in the middle of the lining.

The dynamic stress concentration factor and the map of the maximum acceleration distribution obtained by the two modes of lateral explosion and upper explosion of Figures 1 and 2 present typical symmetrical patterns of butterfly distribution.

The maximum internal force response formula of arbitrary angle on lining is derived under any angle impact load.

First consider the special case of the impacted load on the upper side of the lining; the impact load can be expressed by arbitrary rotating angle; the additional force of lining under impact load is divided into three parts.

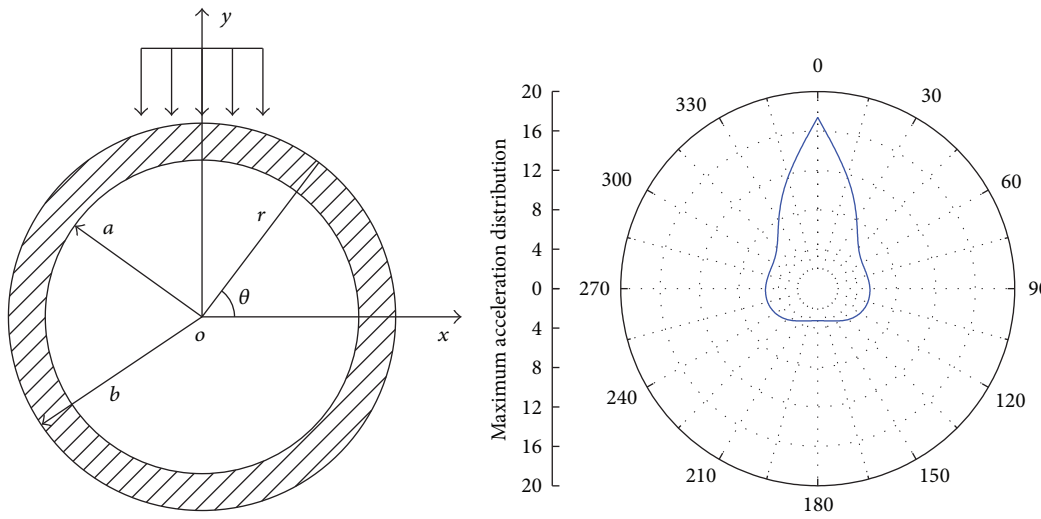

(a) Mechanical model (b) Upper soil blasting the maximum acceleration distribution

Figure 2: Upper blasting load coefficient of dynamic stress distribution of surrounding rock [8].

The first part is the equivalent impact load, with the blasting load applied on the lining; the second part is the equivalent impact reaction force, which is the reverse force of lining and formation, equal to the equivalent impact load for balance effect; the third part is the proposed rock resistance force on both sides of lining; it is caused by the relative displacement mode between the lining and ground.

We give the case study of the triangle resistance distribution; the load model is shown as in Figure 3. The effective counter force which is under the influence of impact in order to maintain the balance of force provided by the formation of lining is equal to the action of the equivalent load and impact load. The distribution of load model can be traced back to the Japanese triangle resistance method [7].

According to the stress characteristics of structure response under impact load, the force model diagram of the circular tunnel lining under the upper blasting impact is given. Two main factors should be considered for affecting the load and the response of the lining under the impact load: load form and load value. Figure 3(a) shows the force model of the circular lining under the condition of impact load. Figure 3(b) is the mechanical model of additional load for blasting shock.

The equivalent action form of impact load is discussed first. There are two loading modes of simulating the blasting and impact loading of rock: one is calculating the explosion hole pressure by explosive burst detonation theory and then loading the calculating blast action on hole wall directly; second is using the empirical formula to calculate the dynamical peak value of the load and then imposing it on the boundary according to triangular pulse wave form. The former method needs to introduce the state equations of the explosive detonation and the rock mass, which is used for single hole blasting or centralized charge blasting. For the impact of porous blasting, the blasting source distribution area is larger; the simulation is not directly loaded with blasting hole pressure according to the equivalent amount of explosives to concentrate on loading and explosive loading. The simulation of blasting vibration effect is based on triangle pulse wave loading [7]. Suppose that the effect of gas outburst, seismic wave, and blasting attenuation on lining is equivalent. The equivalent additional load caused by impact load is assumed to consist of three parts: the upper part load and the two-side reaction force and the bottom reaction force. The influence of the different distribution forms on the internal force of the lining is discussed in three parts. The assumed distribution of the blasting load is shown in Figure 4.

Assume that the impact load produces the same total equivalent value F; the concentration of Figure 4 in four kinds of load on the upper part of the form is (a) < (b) < (c) < (d); Figure 4(d) is the limit form of concentrated load; the impact load can act as the concentrated load. Stress concentration in the middle of the lining is the most significant. The concentration degree of subgrade load under the same condition of the equivalent impact load F is ① < ②.

2.2. The Formula Deduction of Lining Internal Force under Impact Load. The internal force formula of lining response under various forms of equivalent impact load is derived. The force F in the process is the total load value of the impact load. Because the computation processes of internal force calculation for different impact loads combination are similar, the paper gives a detailed derivation of the upper curve load for reference, and the rest of the cases only give the result.

Suppose the upper impact equivalent load is sinusoidal and the maximum value is q_0; the sine load value is $q_0 \cos\xi$ in the angle of ξ, and take the range of $-\theta \sim \theta$ as the load calculation of the equivalent load. When $0 \le \varphi \le \theta$, two load diagrams are shown in Figure 5; the bending moment at φ caused by $d\xi$ is $q_0 \cos\xi R \cos\xi d\xi (R\sin\varphi - R\sin\xi)$, of which $q_0 \cos\xi$ is the load value at $d\xi$, $R\cos\xi d\xi$ is the action scope, and $(R\sin\varphi - R\sin\xi)$ is the action distance.

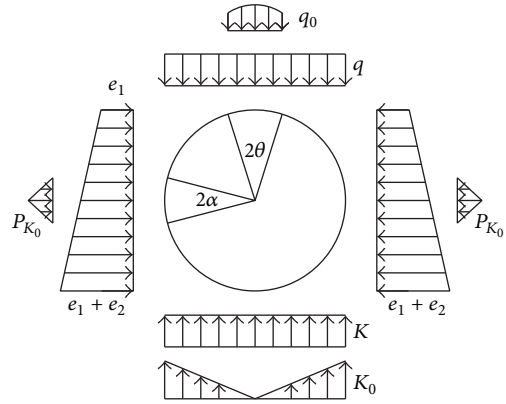

(a) Blasting stress model of upper side

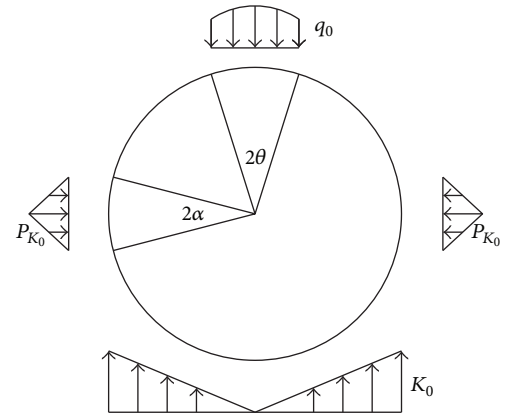

(b) Additional mechanical load model of upper blasting stress

Figure 3: Load model.

While $0 < \varphi \le \theta$,

$$M_{f1} = -\int_0^{\varphi} q_0 \cos\xi R \cos\xi \, d\xi \, (R\sin\varphi - R\sin\xi) = \left(\frac{1}{3} - \frac{1}{2}\sin^2\varphi\cos\varphi - \frac{1}{2}\varphi\sin\varphi - \frac{1}{3}\cos^3\varphi\right) q_0 R^2. \tag{1}$$

The load diagram is shown as in Figure 5, while $\theta < \varphi \le \pi$:

$$M = \left(\frac{1}{3} - \frac{1}{2}\sin^2\theta\cos\theta - \frac{1}{2}\theta\sin\theta - \frac{1}{3}\cos^3\theta\right) q_0 R^2,$$
$$N = \frac{1}{2}(\theta + \sin\theta\cos\theta) q_0 R, \tag{2}$$
$$M_{f2} = \left[\left(\frac{1}{3} - \frac{1}{3}\cos^3\theta\right) - \frac{1}{2}(\theta + \sin\theta\cos\theta)\sin\varphi\right] q_0 R^2.$$

Δ_{1P}, Δ_{2P} can be calculated after the calculation formula of M_F is gotten as

$$\Delta_{1P} = \frac{1}{EJ}\int_0^{\pi} M_F R \, d\varphi = \left(-\frac{1}{2}\theta - \frac{1}{6}\sin^3\theta - \frac{13}{18}\sin\theta - \frac{11}{18}\sin\theta\cos^2\theta + \frac{1}{3}(\theta - \pi)\cos^3\theta + \frac{\pi}{3} - \frac{1}{2}\sin\theta\cos\theta\right)\frac{q_0 R^3}{EJ}, \tag{3}$$
$$\Delta_{2P} = -\frac{R^2}{EJ}\int_0^{\pi} M_F \cos\varphi \, d\varphi = \frac{1}{16}\left[\theta - \sin\theta\cos\theta\left(1 - 2\cos^2\theta\right)\right]\frac{q_0 R^4}{EJ}.$$

Then

$$\delta_{11} = \frac{1}{EJ}\int_0^{\pi} \overline{M}_1^2 R \, d\varphi = \frac{\pi R}{EJ},$$
$$\delta_{22} = \frac{1}{EJ}\int_0^{\pi} \overline{M}_2^2 R \, d\varphi = \frac{\pi R^3}{2EJ},$$
$$x_1 = -\frac{\Delta_{1P}}{\delta_{11}} = -\left[\left(-\frac{1}{2}\theta - \frac{1}{6}\sin^3\theta - \frac{13}{18}\sin\theta - \frac{11}{18}\sin\theta\cos^2\theta + \frac{1}{3}(\theta - \pi)\cos^3\theta + \frac{\pi}{3} - \frac{1}{2}\sin\theta\cos\theta\right)\right]\frac{q_0 R^2}{\pi}, \tag{4}$$
$$x_2 = -\frac{\Delta_{2P}}{\delta_{22}} = -\frac{1}{8\pi}\left[\theta - \sin\theta\cos\theta\left(1 - 2\cos^2\theta\right)\right] q_0 R.$$

Put the values of x_1 and x_2 into $M_{q\varphi} = x_1 - x_2 R\cos\varphi + M_q$.

While $0 \le \varphi \le \theta$,

$$M_{q0\varphi} = -\left[\left(-\frac{1}{2}\theta - \frac{1}{6}\sin^3\theta - \frac{13}{18}\sin\theta - \frac{11}{18}\sin\theta\cos^2\theta + \frac{1}{3}(\theta - \pi)\cos^3\theta + \frac{\pi}{3} - \frac{1}{2}\sin\theta\cos\theta\right)\right]\frac{q_0 R^2}{\pi} + \frac{1}{8\pi}\left[\theta - \sin\theta\cos\theta\left(1 - 2\cos^2\theta\right)\right]\cos\varphi q_0 R^2 + \left(\frac{1}{3} - \frac{1}{2}\sin^2\varphi\cos\varphi - \frac{1}{2}\varphi \cdot \sin\varphi - \frac{1}{3}\cos^3\varphi\right) q_0 R^2. \tag{5}$$

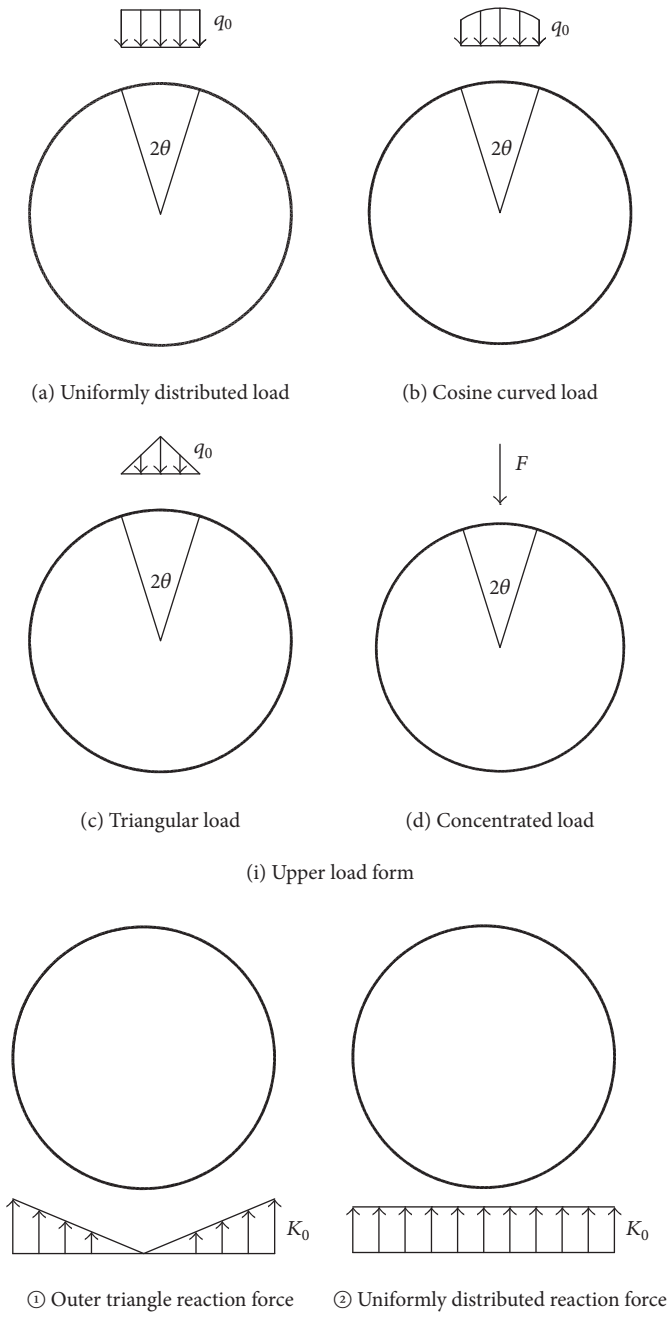

(a) Uniformly distributed load (b) Cosine curved load

(c) Triangular load (d) Concentrated load

(i) Upper load form

① Outer triangle reaction force ② Uniformly distributed reaction force

(ii) Subgrade reaction distribution

FIGURE 4: Blasting load form.

While $\theta < \varphi \le \pi$,

$$M_{q0\varphi} = -\left[\left(-\frac{1}{2}\theta - \frac{1}{6}\sin^3\theta - \frac{13}{18}\sin\theta - \frac{11}{18}\sin\theta\cos^2\theta + \frac{1}{3}(\theta-\pi)\cos^3\theta + \frac{\pi}{3} - \frac{1}{2}\sin\theta\cos\theta\right)\right]\frac{q_0R^2}{\pi} + \frac{1}{8\pi}\left[\theta - \sin\theta\cos\theta\left(1 - 2\cos^2\theta\right)\right]\cos\varphi q_0R^2 + \left[\left(\frac{1}{3} - \frac{1}{3}\cos^3\theta\right) - \frac{1}{2}(\theta + \sin\theta\cos\theta)\sin\varphi\right]q_0R^2. \tag{6}$$

The relationship between the equivalent blasting force F and q_0 is

$$F = (\theta + \sin\theta\cos\theta)\, q_0R. \tag{7}$$

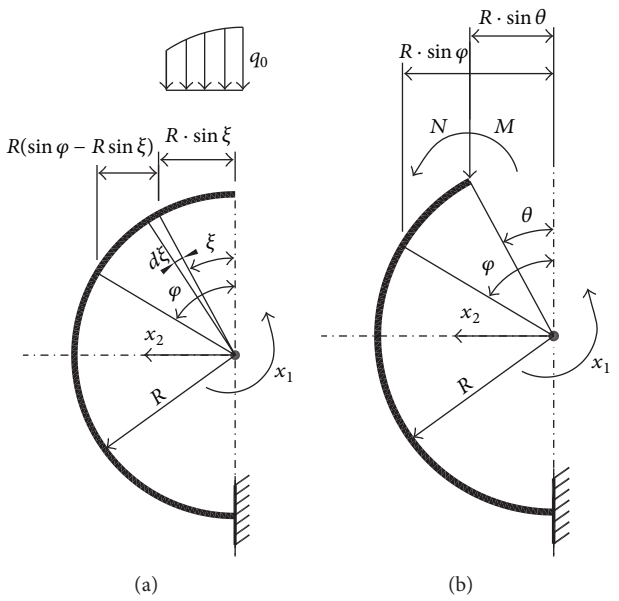

Figure 5: Load diagram of curves (a) and (b).

The axial force calculation is (8), while $0 \le \varphi \le \theta$:

$$N_{q1} = q_0 R \sin\varphi \sin\varphi = \frac{F}{(\theta + \sin\theta\cos\theta)} \sin^2\varphi. \tag{8}$$

While $\theta < \varphi \le \pi$,

$$N_{q2} = q_0 R \sin\theta \sin\varphi = \frac{F\sin\theta}{(\theta + \sin\theta\cos\theta)} \sin\varphi. \tag{9}$$

Bring the values of X_1 and X_2 into $N_{q\varphi} = x_2\cos\varphi + N_q$.

While $0 \le \varphi \le \theta$,

$$N_{q\varphi} = \left[-\frac{1}{8\pi}\left[\theta - \sin\theta\cos\theta\left(1 - 2\cos^2\theta\right)\right]\cos\varphi + \sin^2\varphi\right] \frac{F}{(\theta + \sin\theta\cos\theta)}. \tag{10}$$

While $\theta < \varphi \le \pi$,

$$N_{q\varphi} = \left[-\frac{1}{8\pi}\left[\theta - \sin\theta\cos\theta\left(1 - 2\cos^2\theta\right)\right]\cos\varphi + \sin\theta\sin\varphi\right] \frac{F}{(\theta + \sin\theta\cos\theta)}. \tag{11}$$

The calculation formula of shear force is as follows: while $0 \le \varphi \le \theta$,

$$Q_{q1} = \frac{F}{(\theta + \sin\theta\cos\theta)} \sin\varphi\cos\varphi. \tag{12}$$

While $\theta < \varphi \le \pi$,

$$Q_{q2} = \frac{F\sin\theta}{(\theta + \sin\theta\cos\theta)} \cos\varphi. \tag{13}$$

Bring x_1 and x_2 into $Q_{q\varphi} = x_2\sin\varphi + Q_q$.

While $0 \le \varphi \le \theta$,

$$Q_{q\varphi} = \left[-\frac{1}{8\pi}\left[\theta - \sin\theta\cos\theta\left(1 - 2\cos^2\theta\right)\right]\sin\varphi + \sin\varphi\cos\varphi\right] \frac{F}{(\theta + \sin\theta\cos\theta)}. \tag{14}$$

While $\theta < \varphi \le \pi$,

$$Q_{q\varphi} = \left[-\frac{1}{8\pi}\left[\theta - \sin\theta\cos\theta\left(1 - 2\cos^2\theta\right)\right]\sin\varphi + \sin\theta\cos\varphi\right] \frac{F}{(\theta + \sin\theta\cos\theta)}. \tag{15}$$

The maximum value of instantaneous explosive load and maximum internal force can be obtained by bringing maximum F into the formula.

The expression of maximum explosion pressure is given in 1956 by Brown in the equivalent value of blasting load [1] as

$$P_b = \frac{0.45\rho V^2}{(1.0 + 0.0008\rho)}. \tag{16}$$

1971 Sassa gives the following expressions:

$$P_b = 0.42\rho V^2\left(1 - 0.543\rho + 0.193\rho^2\right). \tag{17}$$

The detonation wave spread in the rock mass gives the maximum pressure $P_{\max}$ in the contact interface of explosive and rock. The maximum pressure $P_{\max}$ generated on the contact interface between the detonation wave and the rock mass is related to the rock physical characteristic. The maximum pressure and the maximum explosion pressure relation can be approximately expressed as follows:

$$P_{\max} = \frac{2\rho C_p}{\rho C_p + V\rho_0} P_b. \tag{18}$$

ρ is rock density; C_p is p wave velocity propagated in rocks; V is explosive detonation velocity; ρ_0 is explosive density.

The maximum equivalent load is

$$F_{\max} = P_{\max}\frac{\pi D^2}{4}. \tag{19}$$

The relationship between the peak value of blasting load and the distance can be expressed as

$$P_c = \frac{D^3}{8r^3} P_{\max}. \tag{20}$$

$P_{\max}$ is peak value of blasting load; r is the distance from the calculate point to blasting hole; D is the diameter of the contact surface (m).

The Statfield dynamic pressure with the time history can be used as

$$P_D(t) = 4P_{\max}\left(e^{-Bt/\sqrt{2}} - e^{-\sqrt{2}Bt}\right), \tag{21}$$

where $B = 163.38$ kPa is the load constant, having an amount equivalent to the dynamic pressure generated by the charge of each 1 kg explosive [1].

The function of equivalent total load value on the lining with the time from formulas (16)–(21) is

$$F(t) = \frac{D^3}{2r^3}\left(e^{-Bt/\sqrt{2}} - e^{-\sqrt{2}Bt}\right)F_{\max}, \tag{22}$$

where $F_{\max}$ is the maximum value of blasting load on the contact lining surface.

The internal force calculated by the different combination of load form is shown in the Appendix.

3. Test Verification of the Model

3.1. Comparison with the Blasting Model Test. In order to further verify the applicability of the theoretical calculation formula of the instantaneous maximum internal force of the circular lining (Figure 4) under the impact load, the calculation and comparison of the microvibration centrifuge model test results on the top of lining are carried out. The top vibration model test diagram is shown in Figure 6.

The parameters of impact load model test on the upper part of the lining are shown in Table 1 [9]. The comparison and analysis of the test results are carried out as follows.

The bending moment of the structure under impact load can be obtained by converting the microstrain model test results. The model tests show that the mix ratio of sand to gypsum material is gypsum plaster material : sand : water = 1 : 0.8 : 0.5; elastic modulus $E = 2.8$ GPa, which is the reduction elasticity modulus of the prototype concrete C20. Compare two kinds of thickness with 7.5 mm and 12.5 mm; the elastic modulus of aluminum alloy model test is $E_m = 70$ Gpa; the thickness is 3.8 mm.

The similarity criterion of bending deformation of the model centrifuge test is as follows:

$$h_m = \frac{h_p}{n}\left[\frac{E_p\left(1-\mu_m^2\right)}{E_m\left(1-\mu_p^2\right)}\right]^{1/3}, \qquad \sigma_p = \frac{h_p}{nh_m}\frac{E_p}{E_m}\sigma_m. \tag{23}$$

n is the number of centrifugal accelerations; μ_m is Poisson's ratio of the model; μ_p is Poisson's ratio of the prototype; E_m is Young's modulus of the model; E_P is Young's modulus of the prototype; h_m is the thickness of the model lining; h_p is the thickness of the prototype lining.

The next formula is available by the formula of (23):

$$\frac{\sigma_p}{\sigma_m}\frac{E_m}{E_p} = \frac{\varepsilon_p}{\varepsilon_m} = \frac{h_p}{nh_m} = \left[\frac{E_m\left(1-\mu_p^2\right)}{E_p\left(1-\mu_m^2\right)}\right]^{1/3}. \tag{24}$$

$\mu_m = \mu_p$ and $E_m = E_p$ are suitable for the sand gypsum material; the moment can be calculated by directly substituting the experimental microstrain into the prototype; for the aluminum alloy material, it can be calculated by

$$\frac{\varepsilon_p}{\varepsilon_m} = \frac{h_p}{nh_m} = \frac{265}{50\times 3.8} = \frac{1.4}{1}. \tag{25}$$

According to the formula of $M = W_z\sigma_{\max} = (bh^2/6)\varepsilon_{\max}E_{\mathrm{mix}}$, the instantaneous maximum bending moment of the prototype can be obtained. The elasticity modulus of the prototype concrete is $E_{\mathrm{mix}} = 28$ GPa. The results of converted moment value of the measuring point are shown in Table 2.

The equivalent blasting load values are calculated by the third groups of experiments, and the parameters of the

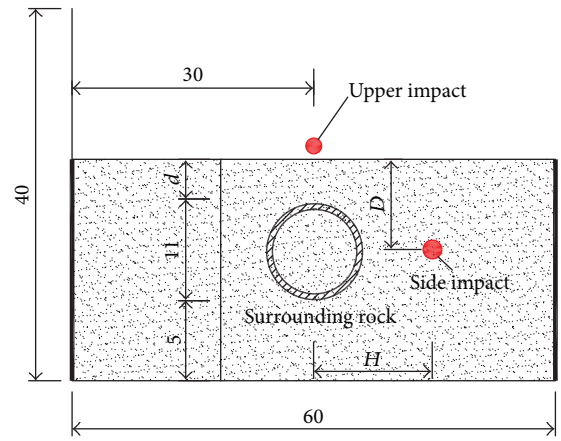

Figure 6: Schematic diagram of microvibration test [9].

Table 1: Parameters of model test.

Serial number	Density of surrounding rock g/cm^3	Explosive quantity g	Blasting distance cm
3 (top explosion)	1.613	1.25	5.5
4 (top explosion)	1.633	1.25	3
5 (top explosion)	1.633	2.5	3
6 (top explosion)	1.649	1.25	3
31 (side explosion)	1.65	1.25	12.5
34 (side explosion)	1.65	2.5	30

Table 2: The converted moment value of the measuring point.

	Measuring point 1	Measuring point 2	Measuring point 3	Measuring point 4
3	324.2	−149.7	119.6	−154.0
4	255.2	−93.7	77.6	−81.9
5	717.1	−346.8	249.9	−247.7
6	369.5	−121.7	122.8	−134.7
31	−144.2	380.5	−189	181.9
34	−136.6	130.7	−78.3	88.5

Table 3: Test parameters.

Test number	Density of surrounding rock g/cm^3	Explosive quantity g	Cover thickness cm	Explosive density g/cm^3	Detonation velocity of black powder m/s	Shear wave velocity of rock m/s	Diameter of explosive column mm
3	1.613	2.5	3	1.63	500	154.8	11

test are shown in Table 3 [9]. The theoretical solution of maximum internal force to test model is calculated.

Then

$$P_b = \frac{0.45\rho V^2}{(1.0 + 0.0008\rho)} = 140.5\,\text{MPa},$$

$$P_{\max} = \frac{2\rho C_p}{\rho C_p + V\rho_0} P_b = 65.6\,\text{MPa}, \tag{26}$$

$$F_{\max} = P_{\max}\frac{\pi D^2}{4} = 6.23\,\text{kN}.$$

The attenuated equivalent load is $F = D^3/8r^3 \times F_{\max}$ by giving $P_c = D^3/8r^3 \times P_{\max}$ according to the test conditions; the conversion coefficient of black powder and TNT is 0.4; the centrifugal acceleration is 50 g; then 1.25 g black powder is equivalent to TNT of 62.5 kg [9]; then

$$F_5 = \frac{11^3}{8 \times 55^3} \times 6.23 \times 125000 = 778\,\text{kN}. \tag{27}$$

That means the equivalent blasting load on the lining of third groups experimental results is 778 kN, considering that the size effect of model test will lead to error; the selection range of calculation load is from 600 kN to 800 kN.

The internal force of the maximum impact load for the circular lining under the condition of the load combination is calculated as shown in Figure 7. The equivalent form of the upper impact load is compared with the uniform load, the curve load, the triangle load, and the concentrated load. The concentrated load represents the extreme case where the impact load directly acts on the lining without attenuation through the surrounding rock.

Select the different calculation combination of blasting load form in the top and bottom; the results are compared as shown in Tables 4–9; take $\theta = 15^\circ, \alpha = 45^\circ$. The comparison of the scatter plots is shown in Figure 7.

The following can be concluded through comparison of a①, b①, c①, and d①:

(1) The influence of the upper load form on the bending moment of the measuring point 1 (top) is obvious, the difference range can reach 50%–100%, and the comparison of the load distribution is very necessary.

(2) The characteristics of each group showed a clear trend of convergence; the measured moment value of point 1 represents the relationship a① < b① < c① < d①. This shows that with more concentration in the upper part of the load form the moment value of measuring point 1 will be greater.

(3) Compared with each test point data under all cases of combination, it can be known that the measuring points of the bending moment values have changed

Table 4: Calculation comparison of test groups 3.

	Test	a①	b①	c①	d①	b②
1	324.2	207.9	330.8	367.2	436.9	352.0
2	−149.7	−259.8	−174.6	−173.5	−178.5	−198.1
3	119.6	−16.1	135.1	132.7	134.3	209.4
4	−154.0	−259.8	−174.6	−173.5	−178.5	−198.1

Note: the equivalent blasting load is 630 kN; the lateral resistance force is 56 kN/m.

Table 5: Calculation comparison of test groups 4.

	Test	a①	b①	c①	d①	b②
1	255.2	148.3	254.8	286.3	346.8	273.1
2	−93.7	−184.7	−110.7	−109.8	−114.1	−131.0
3	77.6	−45.9	85.3	83.0	84.4	149.7
4	−81.9	−184.7	−110.7	−109.8	−114.1	−131.0

Note: the equivalent blasting load is 546 kN; the lateral resistance force is 84 kN/m.

Table 6: Calculation comparison of test groups 5.

	Test	a①	b①	c①	d①	b②
1	717.1	473.2	746.5	827.3	982.2	793.4
2	−346.8	−591.8	−402.4	−399.7	−410.9	−454.3
3	249.9	−24.5	311.5	306.0	309.7	476.7
4	−247.7	−591.8	−402.4	−399.7	−410.9	−454.3

Note: the equivalent blasting load is 1400 kN; the lateral resistance force is 112 kN/m.

Table 7: Calculation comparison of test groups 6.

	Test	a①	b①	c①	d①	b②
1	369.5	218.5	355.0	395.5	472.9	371.6
2	−121.7	−271.9	−177.2	−175.8	−181.4	−195.2
3	122.8	3.2	171.2	168.6	170.2	213.1
4	−134.7	−271.9	−177.2	−175.8	−181.4	−195.2

Note: the equivalent blasting load is 700 kN; the lateral resistance force is 84 kN/m.

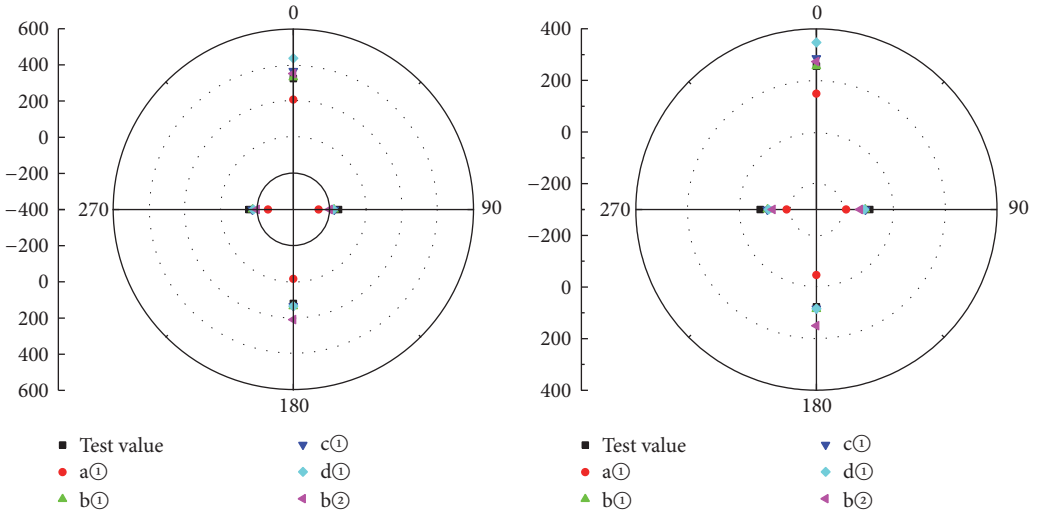

(a) Test group of number 3

(b) Test group of number 4

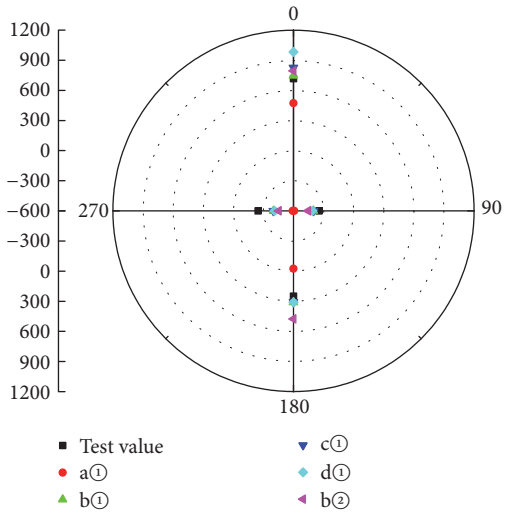

(c) Test group of number 5

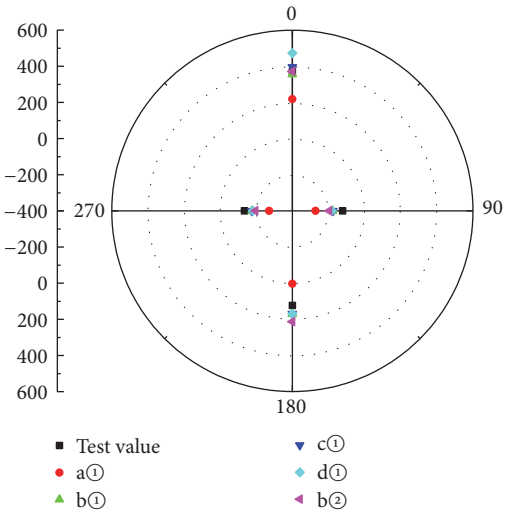

(d) Test group of number 6

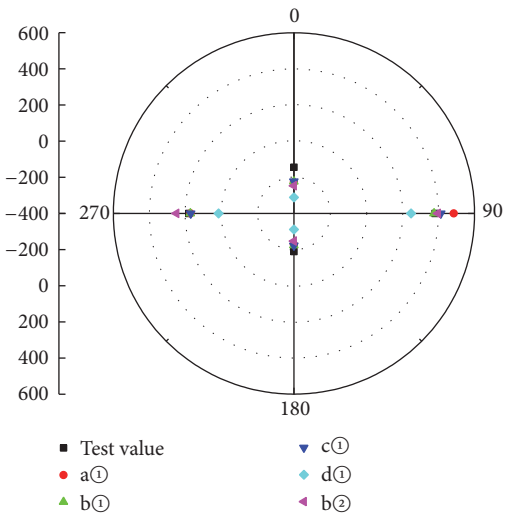

(e) Test group of number 31

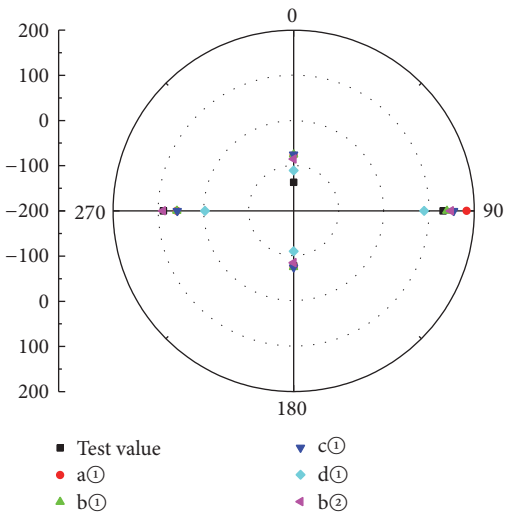

(f) Test group of number 34

Figure 7: Comparison of experimental results to model solution.

Table 8: Calculation comparison of test groups 4.

	Test	a①	b①	c①	d①	b②
1	−144.2	−227.4	−223.4	−222.2	−311.4	−247.5
2	380.5	484.8	375.3	412.9	248.5	397.2
3	−189	−227.4	−223.4	−222.2	−311.4	−247.5
4	181.9	172.5	173.4	170.9	17.4	250.1

Note: the equivalent blasting load is 650 kN; the lateral resistance force is 20 kN/m.

Table 9: Calculation comparison of test groups 34.

	Test	a①	b①	c①	d①	b②
1	−136.6	−77.2	−75.6	−75.1	−110.8	−85.3
2	130.7	183.1	139.3	154.4	88.6	148.1
3	−78.3	−77.2	−75.6	−75.1	−110.8	−85.3
4	88.5	58.2	58.6	57.5	−3.8	89.2

Note: the equivalent blasting load is 260 kN; the lateral resistance force is 20 kN/m.

considerably when the upper load form changed from the uniform load to the curve load. The rule is that the measuring point 1 and point 3 (the top and bottom points of the lining) bending moment value increases and the measuring point 2 and point 4 (the point on left-right sides of the lining) bending moment value decreases.

(4) Compared with each test point data of 2, 3, and 4 under all cases of combination of b①, c①, and d①, it can be known that the increase concentration of the upper load and the linear increase effect of the internal force response are decreased. The effect of concentration on both sides and the bottom of the lining is very weak (within 1%).

Compared with the test combination of b① and b②, the result showed the following:

(1) The form influence of the ground reaction force on the moment of the measuring point 1 (bottom) is obvious, and the difference range is 90%–50%.

(2) The difference range of the combination of b① and b② is larger (range: 10%–50%) for the measuring point 1, point 2, and point 4. This shows that the concentration increase of the subgrade force in the bottom of lining will only affect the bending moment of the action position and have less effect on the other points' bending moment outside of this range.

Comparing the data calculation in the four groups, it is found that the combination of upper triangular load and subgrade counterforce of the outer triangle reaction model has good coincidence degree with the experimental values. This case also has the certain safety reserve; comparatively, this load combination is the most reasonable one. The internal force calculation results (bending moment, shear force, and axial force) of the upper triangular load and the subgrade counterforce of outer triangle reaction model are shown in Figure 8.

Validating the lining safety theoretical results of the third test groups preliminarily, the calculation results of triangular equivalent loads are selected to verify the results, while the maximum value of the calculated moment is 367.2 kN m, the position is S1 measuring point, and the axial force is 247.8 kN.

According to the maximum compressive classical stress formula of the eccentric compression member,

$$\sigma_{\max} = \frac{N}{A} + \frac{M}{W_Z}. \tag{28}$$

Bring the test parameters and calculation results; the following can be concluded:

$$\varepsilon_{\max} = \frac{\sigma_{\max}}{E_C} = \frac{1}{E_C}\left(\frac{N}{A} + \frac{M}{W_Z}\right) = 0.00115. \tag{29}$$

The compressive strain is considered as the critical value. The lining structure can be considered in a safe condition as $\varepsilon_{\max}$ less than the concrete elastic ultimate compressive strain of 0.002.

The compression plane strain of the test results is

$$\varepsilon = (0.000706 + 0.00005) \times 1.4 = 0.00106 < 0.002. \tag{30}$$

It can be considered that the lining structure is in a safe state under the case study of blasting load.

3.2. Comparison to Model Test of Pneumatic Impact Load. Compare the pneumatic impact load mode to the model test. The test model box is shown as in Figure 9(a) [10]. The air tube is located in the three (left, right, and down) directions of the model box. The air pressure is equivalent to the triangular load. The additional load is caused by air pressure and the equivalent loading is shown in Figure 9(b). The upper uniformly distributed load is the subgrade counterforce provided by the equilibrium pressure from the lower pressure layer.

The comparison of the additional bending moment and the theoretical calculation results of the lining structure under releasing and applying air pressure to the test is shown in Table 10.

It is found that the calculation results of the additional bending moment for the circular lining under the impact pressure were coincident with the model test data. Four points' precision accuracy is within 15%, with the highest accuracy reaching 95%. The results for the theory of structure response (Figure 3) moment under impact load calculation results are in good agreement with the experimental values. It can provide support for theoretical calculation of tunnel lining structure response under impact loading.

4. Numerical Simulation to Microvibration Test

MIDAS GTS was used to simulate the microvibration model test. After the model feature was calculated, the response simulation of lining (Figure 3) under blasting load was carried out by using the time history analysis.

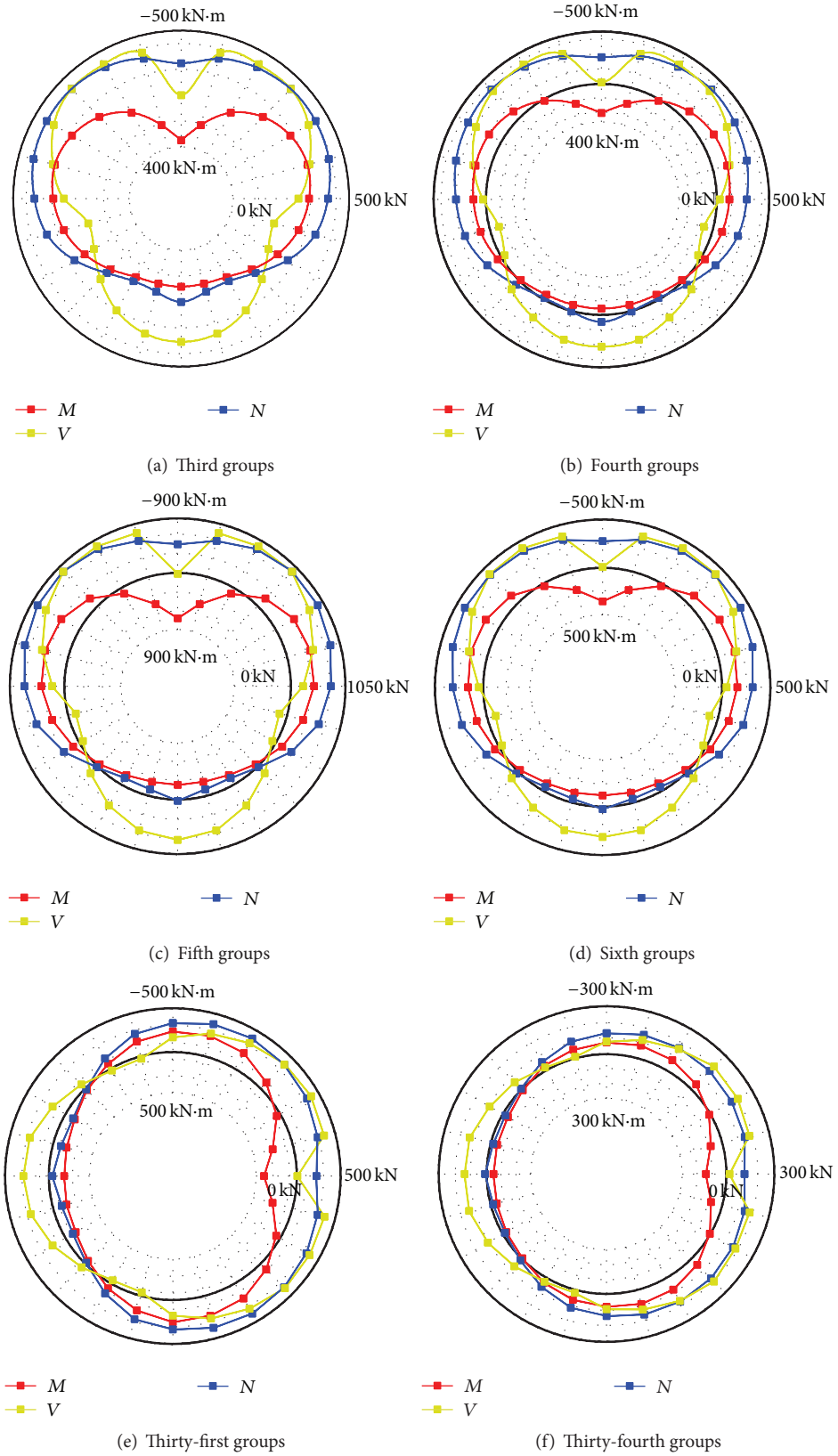

Figure 8: Comparison results of bending moment, shear force, and axial force.

Table 10: Comparison of the bending moment for the pneumatic impact loading on structure.

Measuring point	Air pressure releasing		Air pressure applying	
	Test value	Calculated value	Test value	Calculated value
X6	−0.86	−0.84	−1.1	−0.63
X7	1.68	1.63	1.3	1.22
X8	1.83	−8.68	0.76	−6.51
X9	−2.26	7.08	−0.52	5.31
X10	−1.17	1.99	−0.43	1.49

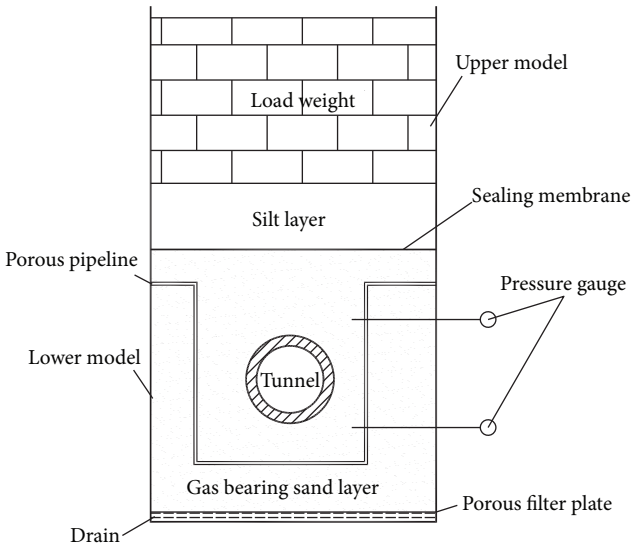

(a) Model test [10]

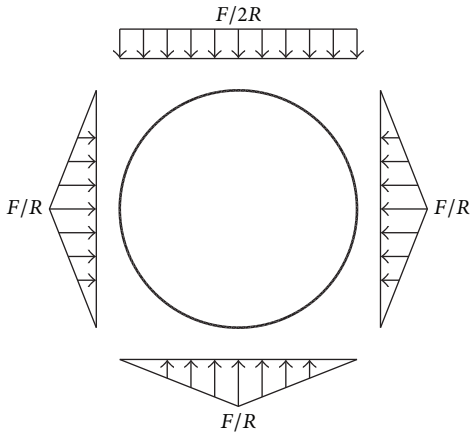

(b) Equivalent loading of air pressure

Figure 9: Blasting loading.

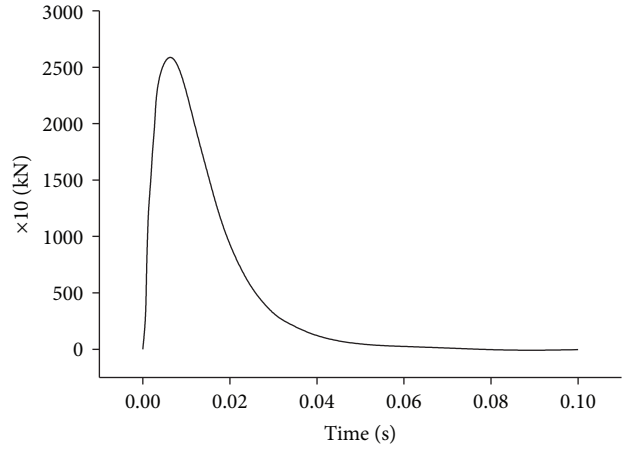

Figure 10: Dynamic pressure function.

Table 11: Parameters of cohesive soil layer.

Dry density (g/cm^3)	Shear modulus (MPa)	Cohesion (kPa)	Internal friction angle
1.45	0.292	28	29.8°

Table 12: Explosive parameter.

Density (g/cm^3)	Detonation velocity (m/s)	Detonation pressure (GPa)	Elastic modulus (GPa)
1.63	6930	21	4.0

First, the material parameters are given in Tables 11 and 12 [10].

Using MIDAS GTS to simulate the blasting load, manually input the blasting load function. The dynamic pressure time history functions are shown in Figure 10. The blasting load is applied on the interface in form of the surface pressure.

Table 13 [10] shows the maximum microstrain simulation value of the lining structure under blasting loads in consistency with the test value very well; most of the gap is less than 30%. Most difference of the measuring points is less than 30%. The numerical simulation results not only verify the experimental results but also provide the basis for the correctness of the theoretical calculation results. Compared with the results of numerical simulation, the theoretical formula of the lining maximum internal force under impact loading has good applicability in the case study.

Using the GTS, simulate and validate test results; the impact pseudostatic load simulations are carried out by constrained lining structure of tunnel lining by the spring boundary. Theoretically, the simulation and experimental results are compared with the results shown in Table 14. The three-coincidence degree is good through comparison; most difference of the points is less than 20%. The applicability of

Table 13: Comparison of measured point bending strain values to simulation data (%).

Group number		Test point 1	Test point 2	Test point 3	Test point 4
3	A	−706.6	326.3	−260.6	335.7
	B	−534.3	145.7	−142.9	197.1
4	A	−556.4	204.2	−169.0	178.4
	B	−1057.1	196.4	−207.1	264.3
5	A	−1563.0	755.9	−544.6	539.9
	B	−2114.3	392.9	−414.3	528.6
6	A	−805.2	265.3	−267.6	293.4
	B	−964.3	207.1	−214.3	267.9
31	A	432.4	−1141	566.8	−545.6
	B	969.3	−1251.4	694.6	−650.0
34	A	408.8	−392	234.8	−265.3
	B	391.1	−406.8	324.6	−304.3

Note: A for the test results; B for simulation results.

Table 14: Comparison of bending moment (M/kN).

Measurement number		Test point 1	Test point 2	Test point 3	Test point 4
3.0	A	324.2	−149.7	119.6	−154
	B	367.2	−173.5	132.7	−173.5
	C	347.3	−161.1	113.7	−161.1
4	A	255.2	−93.7	77.6	−81.9
	B	286.3	−109.8	83	−109.8
	C	271.9	−102.6	69.4	−102.6
5	A	717.1	−346.8	249.9	−247.7
	B	827.3	−399.7	306	−399.7
	C	782.2	−371.2	263.1	−371.2
6	A	369.5	−121.7	122.8	−134.7
	B	395.5	−175.8	168.6	−175.8
	C	368	−156.3	108.5	−156.3
31	A	−144.2	380.5	−189	181.9
	B	−222.2	412.9	−222.2	170.9
	C	−205.8	389.3	−205.8	148.4
34	A	−136.6	130.7	−78.3	88.5
	B	−75.1	154.4	−75.1	57.5
	C	−69.9	146	−69.9	49.5

Note: A is the experimental result, B is the result of the calculation, and C is the simulation result.

the theoretical calculation results is verified further by the results of impact pseudostatic load simulation.

5. Conclusions

Impact pseudostatic load equivalent model and the maximum internal force solution for circular tunnel lining structure were deduced from classical theory of the free deformation method. The equivalent model and the maximum internal force solution of the underground lining are given. The equivalent load forms of different impact loads are compared preliminarily. The following conclusions and recommendations of the maximum internal force of lining structure under impact load may also be drawn by comparing the theoretical solution, experimental data, and numerical simulation results.

(1) The equivalent form of impact load has a remarkable influence on the calculation results. It was reflected in the internal forces distribution pattern of the lining structure in the load range of impact pseudostatic action.

Two equivalent forms of impact loading on the lining structure of tunnel lining were compared by the curve distributed shape and triangle distributed shape. The simplified triangular distributed load is more convenient and feasible to use with the premise of closing the test results.

(2) The additional load caused by the impact load mainly has two types, the ground counterforce and lateral deformation resistance, which can be calculated by the classical Japanese triangle resistance method. The equivalent mode of formation reaction has two modes, which are external triangle distribution and uniform distribution. For the case of side impact load, the distribution of the outer triangle is obviously better than that of the uniform distribution load distribution, whether from the dynamic stress concentration degree of the surrounding ground or from the matching degree to test data.

(3) The influence of soil parameters on the structural lining response under blasting shock load is the following: the soil density influences the transmission and attenuation of shock wave in surrounding rock and the formation parameters for the effect of structural response under blasting load: soil density influences the detonation wave in the soil layer of propagation and attenuation. The characteristics show that the lower the density, the softer the soil and the more significant attenuation of impact loads. The distance between blasting spot and lining structure is similar to the factor of the soil layer density; the farther the distance, the faster

Table 15: Summary table of the moment formula.

Load	Range	Moment value
Equivalent load of curve impact	$\varphi = 0 \sim \theta$	$M_{q0\varphi} = \frac{D^3}{2r^3}\left(e^{-Bt/\sqrt{2}} - e^{-\sqrt{2}Bt}\right)\frac{F_{\max}R}{(\theta + \sin\theta\cos\theta)}\left[-\left[\left(-\frac{1}{2}\theta - \frac{1}{6}\sin^3\theta - \frac{13}{18}\sin\theta - \frac{11}{18}\sin\theta\cos^2\theta + \frac{1}{3}(\theta - \pi)\cos^3\theta + \frac{\pi}{3} - \frac{1}{2}\sin\theta\cos\theta\right)\right]\frac{1}{\pi} + \frac{1}{8\pi}\left[\theta - \sin\theta\cos\theta\left(1 - 2\cos^2\theta\right)\right]\cos\varphi + \left(\frac{1}{3} - \frac{1}{2}\sin^2\varphi\cos\varphi - \frac{1}{2}\varphi\sin\varphi - \frac{1}{3}\cos^3\varphi\right)\right]$
	$\varphi = \theta \sim \pi$	$M_{q0\varphi} = \frac{D^3}{2r^3}\left(e^{-Bt/\sqrt{2}} - e^{-\sqrt{2}Bt}\right)\frac{F_{\max}R}{(\theta + \sin\theta\cos\theta)}\left[-\left[\left(-\frac{1}{2}\theta - \frac{1}{6}\sin^3\theta - \frac{13}{18}\sin\theta - \frac{11}{18}\sin\theta\cos^2\theta + \frac{1}{3}(\theta - \pi)\cos^3\theta + \frac{\pi}{3} - \frac{1}{2}\sin\theta\cos\theta\right)\right]\frac{1}{\pi} + \frac{1}{8\pi}\left[\theta - \sin\theta\cos\theta\left(1 - 2\cos^2\theta\right)\right]\cos\varphi + \left[\left(\frac{1}{3} - \frac{1}{3}\cos^3\theta\right) - \frac{1}{2}(\theta + \sin\theta\cos\theta)\sin\varphi\right]\right]$
Equivalent load of triangle impact	$\varphi = 0 \sim \frac{\pi}{12}$	$M_{F\varphi} = \frac{D^3}{2r^3}\left(e^{-Bt/\sqrt{2}} - e^{-\sqrt{2}Bt}\right) \times 3.86F_{\max}R\left(0.0715 + 0.00046\cos\varphi - 0.5\sin^2\varphi + 0.644\sin^3\varphi\right)$
	$\varphi = \frac{\pi}{12} \sim \pi$	$M_{q\varphi} = \frac{D^3}{2r^3}\left(e^{-Bt/\sqrt{2}} - e^{-\sqrt{2}Bt}\right) \times 3.86F_{\max}R\left(0.0826 + 0.00046\cos\varphi - 0.129\sin\varphi\right)$
Equivalent load of uniform impact	$\varphi = 0 \sim \theta$	$M_{F\varphi} = \frac{R}{2\sin\theta}\left[\frac{1}{4\pi}\left(3\sin\theta\cos\theta + \theta - 2\sin^2\theta(\pi - \theta) + 4\sin\theta\right) + \frac{\sin^3\theta}{3\pi}\cos\varphi - \frac{1}{2}\sin^2\varphi\right]\frac{D^3}{2r^3}\left(e^{-Bt/\sqrt{2}} - e^{-\sqrt{2}Bt}\right)F_{\max}$
	$\varphi = \theta \sim \pi$	$M_{q\varphi} = \frac{R}{2\sin\theta}\left[\frac{1}{4\pi}\left(3\sin\theta\cos\theta + \theta + 2\theta\sin^2\theta + 4\sin\theta\right) + \frac{\sin^3\theta}{3\pi}\cos\varphi - \sin\theta\sin\varphi\right]\frac{D^3}{2r^3}\left(e^{-Bt/\sqrt{2}} - e^{-\sqrt{2}Bt}\right)F_{\max}$
Equivalent load of concentrated impact	$\varphi = 0 \sim \pi$	$M_{\varphi} = \frac{D^3}{2r^3}\left(e^{-Bt/\sqrt{2}} - e^{-\sqrt{2}Bt}\right)F_{\max}R\left(0.318 - 0.5\sin\varphi\right)$
Resistance of lateral impact	$\varphi = 0 \sim \frac{\pi}{2} - \alpha$	$M_{pk0\varphi} = P_{k0}R^2\left[\frac{((3/4)\alpha\sin\alpha - (11/72)\cos 3\alpha + (3/8)\cos\alpha - (1/12)\alpha\sin 3\alpha - 2/9)}{\pi\sin\alpha} - \frac{(1 - \cos 2\alpha)}{4\sin\alpha}\cos\varphi\right]\left(e^{-Bt/\sqrt{2}} - e^{-\sqrt{2}Bt}\right)$
	$\varphi = \frac{\pi}{2} - \alpha \sim \pi$	$M_{pk0\varphi} = P_{k0}R^2\left[\frac{((3/4)\alpha\sin\alpha - (11/72)\cos 3\alpha + (3/8)\cos\alpha - (1/12)\alpha\sin 3\alpha - 2/9)}{\pi\sin\alpha} - \frac{(1 - \cos 2\alpha)}{4\sin\alpha}\cos\varphi - \left(-\frac{1}{3} + \frac{1}{3}\cos^2\alpha + \frac{1}{2}\sin^2\alpha - \frac{1}{2}\sin\alpha\cos\varphi - \frac{1}{6}\frac{\cos^3\varphi}{\sin\alpha} + \frac{1}{2}\cos^2\varphi\right)\right]\left(e^{-Bt/\sqrt{2}} - e^{-\sqrt{2}Bt}\right)$
Opposite force distribution of triangle	$\varphi = 0 \sim \frac{\pi}{2}$	$M_{K\varphi} = \frac{D^3}{2r^3}\left(e^{-Bt/\sqrt{2}} - e^{-\sqrt{2}Bt}\right)F_{\max}R\left(0.0429 - 0.0796\cos\varphi\right)$
	$\varphi = \frac{\pi}{2} \sim \pi$	$M_{K\varphi}\frac{D^3}{2r^3}\left(e^{-Bt/\sqrt{2}} - e^{-\sqrt{2}Bt}\right)F_{\max}R\left(-0.291 - 0.0796\cos\varphi + 0.5\sin\varphi - 0.167\sin^3\varphi\right)$
Opposite force distribution of uniform	$\varphi = 0 \sim \frac{\pi}{2}$	$M_{K\varphi} = \frac{D^3}{2r^3}\left(e^{-Bt/\sqrt{2}} - e^{-\sqrt{2}Bt}\right)F_{\max}R\left(0.0285 - 0.053\cos\varphi\right)$
	$\varphi = \frac{\pi}{2} \sim \pi$	$M_{K\varphi} = \frac{D^3}{2r^3}\left(e^{-Bt/\sqrt{2}} - e^{-\sqrt{2}Bt}\right)F_{\max}R\left(-0.2215 + 0.5\sin\varphi - 0.053\cos\varphi - 0.25\sin^2\varphi\right)$

the impact load decay rate. The magnitude of the impact load directly affects the response of the lining; the strain of the structure lining presents a nonlinear increasing relationship under the nonlinear interaction to the surrounding ground.

(4) Comparing the theoretical formula and dynamic load simulation to the microvibration test data, the theoretical results of the impact pseudostatic load equivalent model are verified again by the numerical simulation of the equivalent static load.

The results show that the consistency of the test results, theoretical results, and the simulation results of impact pseudostatic load is very high. Most of the difference point is within 20%, which shows that the theoretical calculation results of the proposed model have good applicability.

The maximum microstrain simulation by the dynamic load on lining is in agreement with the test values very well, with most of the difference points being within the range of 30%. The comparison between the experimental results and the theoretical calculation results of the pressure shock load model is carried out; the difference of the closest point is 2.3%.

In conclusion, the impact pseudostatic load equivalent model is proposed for dynamic response analysis of tunnel lining structure. Good agreement among the theoretical analysis, test data, and the simulation is achieved, which preliminarily validates the present model and method.

Table 16: Summary table of the axial force formula.

Load	Range	Axial force value
Equivalent load of curve impact	$\varphi = 0 \sim \theta$	$N_{q\varphi} = \frac{D^3}{2r^3}\left(e^{-Bt/\sqrt{2}} - e^{-\sqrt{2}Bt}\right)\frac{F_{\max}}{(\theta + \sin\theta\cos\theta)}\left[-\frac{1}{8\pi}\left[\theta - \sin\theta\cos\theta\left(1 - 2\cos^2\theta\right)\right]\cos\varphi + \sin^2\varphi\right]$
	$\varphi = \theta \sim \pi$	$N_{q\varphi} = \frac{D^3}{2r^3}\left(e^{-Bt/\sqrt{2}} - e^{-\sqrt{2}Bt}\right)\frac{F_{\max}}{(\theta + \sin\theta\cos\theta)}\left[-\frac{1}{8\pi}\left[\theta - \sin\theta\cos\theta\left(1 - 2\cos^2\theta\right)\right]\cos\varphi + \sin\theta\sin\varphi\right]$
Equivalent load of triangle impact	$\varphi = 0 \sim \frac{\pi}{12}$	$N_{q\varphi} = \frac{D^3}{2r^3}\left(e^{-Bt/\sqrt{2}} - e^{-\sqrt{2}Bt}\right) \times 3.86F_{\max}\left[-0.00046\cos\varphi + \left(1 - 1.93\sin\varphi\right)\sin^2\varphi\right]$
	$\varphi = \frac{\pi}{12} \sim \pi$	$N_{q\varphi} = \frac{D^3}{2r^3}(e^{-Bt/\sqrt{2}} - e^{-\sqrt{2}Bt}) \times 3.86F_{\max}[-0.00046\cos\varphi + 0.129\sin\varphi]$
Equivalent load of uniform impact	$\varphi = 0 \sim \theta$	$N_{q\varphi} = \frac{D^3}{2r^3}(e^{-Bt/\sqrt{2}} - e^{-\sqrt{2}Bt})F_{\max}(-\frac{\sin^2\theta}{6\pi}\cos\varphi + \frac{1}{2\sin\theta}\sin^2\varphi)$
	$\varphi = \theta \sim \pi$	$N_{q\varphi} = \frac{D^3}{2r^3}\left(e^{-Bt/\sqrt{2}} - e^{-\sqrt{2}Bt}\right)F_{\max}\left(-\frac{\sin^2 qR}{6\pi}\cos\varphi + \frac{1}{2}\sin\varphi\right)$
Equivalent load of concentrated impact	$\varphi = 0 \sim \pi$	$N_{\varphi} = 0.5\frac{D^3}{2r^3}\left(e^{-Bt/\sqrt{2}} - e^{-\sqrt{2}Bt}\right)F_{\max}\sin\varphi$
Resistance of lateral impact	$\varphi = 0 \sim \frac{\pi}{2} - \alpha$	$N_{\varphi} = \frac{(1 - \cos 2\alpha)}{4\sin\alpha}P_{k0}R\cos\varphi\left(e^{-Bt/\sqrt{2}} - e^{-\sqrt{2}Bt}\right)$
	$\varphi = \frac{\pi}{2} - \alpha \sim \pi$	$N_{\varphi} = \left(e^{-Bt/\sqrt{2}} - e^{-\sqrt{2}Bt}\right)\left[\frac{(1 - \cos 2\alpha)}{4\sin\alpha}P_{k0}R\cos\varphi - \frac{1}{2}P_{k0}R\left(1 - \frac{\cos\varphi}{\sin\alpha}\right)(\sin\alpha - \cos\varphi)\cos\varphi\right]$
Opposite force distribution of triangle	$\varphi = 0 \sim \frac{\pi}{2}$	$N_{K\phi} = \frac{1}{4\pi}\frac{D^3}{2r^3}\left(e^{-Bt/\sqrt{2}} - e^{-\sqrt{2}Bt}\right)F_{\max}\cos\varphi$
	$\varphi = \frac{\pi}{2} \sim \pi$	$N_{K\phi} = \frac{D^3}{2r^3}\left(e^{-Bt/\sqrt{2}} - e^{-\sqrt{2}Bt}\right)F_{\max}\left(\frac{1}{4\pi}\cos\varphi - \sin\varphi\cos^2\varphi\right)$
Opposite force distribution of uniform	$\varphi = 0 \sim \frac{\pi}{2}$	$N_{K\phi} = 0.053\frac{D^3}{2r^3}\left(e^{-Bt/\sqrt{2}} - e^{-\sqrt{2}Bt}\right)F_{\max}\cos\varphi$
	$\varphi = \frac{\pi}{2} \sim \pi$	$N_{K\phi} = \frac{D^3}{2r^3}\left(e^{-Bt/\sqrt{2}} - e^{-\sqrt{2}Bt}\right)F_{\max}\left(0.5\sin^2\varphi - 0.5\sin\varphi + 0.053\cos\varphi\right)$

Table 17: Summary table of the shear force formula.

Load	Range	Shear value
Equivalent load of curve impact	$\varphi = 0 \sim \theta$	$Q_{q\varphi} = \frac{D^3}{2r^3}\left(e^{-Bt/\sqrt{2}} - e^{-\sqrt{2}Bt}\right)\frac{F_{\max}}{(\theta + \sin\theta\cos\theta)}\left[-\frac{1}{8\pi}\left[\theta - \sin\theta\cos\theta\left(1 - 2\cos^2\theta\right)\right]\sin\varphi + \sin\varphi\cos\varphi\right]$
	$\varphi = \theta \sim \pi$	$Q_{q\varphi} = \frac{D^3}{2r^3}\left(e^{-Bt/\sqrt{2}} - e^{-\sqrt{2}Bt}\right)\frac{F_{\max}}{(\theta + \sin\theta\cos\theta)}\left[-\frac{1}{8\pi}\left[\theta - \sin\theta\cos\theta\left(1 - 2\cos^2\theta\right)\right]\sin\varphi + \sin\theta\cos\varphi\right]$
Equivalent load of triangle impact	$\varphi = 0 \sim \frac{\pi}{12}$	$Q_{q\varphi} = \frac{D^3}{2r^3}\left(e^{-Bt/\sqrt{2}} - e^{-\sqrt{2}Bt}\right) \times 3.86F_{\max}\left[-0.00046\sin\varphi + \left(1 - 1.93\sin\varphi\right)\sin\varphi\cos\varphi\right]$
	$\varphi = \frac{\pi}{12} \sim \pi$	$Q_{q\varphi} = \frac{D^3}{2r^3}\left(e^{-Bt/\sqrt{2}} - e^{-\sqrt{2}Bt}\right) \times 3.86F_{\max}\left[-0.00046\sin\varphi + 0.129\cos\varphi\right]$
Equivalent load of uniform impact	$\varphi = 0 \sim \theta$	$Q_{q\varphi} = \frac{D^3}{2r^3}\left(e^{-Bt/\sqrt{2}} - e^{-\sqrt{2}Bt}\right)F_{\max}\left(-\frac{\sin^2\theta}{6\pi}\sin\varphi + \frac{1}{2\sin\theta}\sin\varphi\cos\varphi\right)$
	$\varphi = \theta \sim \pi$	$Q_{q\varphi} = \frac{D^3}{2r^3}\left(e^{-Bt/\sqrt{2}} - e^{-\sqrt{2}Bt}\right)F_{\max}\left(-\frac{\sin^2\theta}{6\pi}\sin\varphi + \frac{1}{2}\cos\varphi\right)$
Equivalent load of concentrated impact	$\varphi = 0 \sim \pi$	$Q_{\varphi} = -0.5\frac{D^3}{2r^3}\left(e^{-Bt/\sqrt{2}} - e^{-\sqrt{2}Bt}\right)F_{\max}\cos\varphi$
Resistance of lateral impact	$\varphi = 0 \sim \frac{\pi}{2} - \alpha$	$Q_{pk\varphi} = \frac{(1 - \cos 2\alpha)}{4\sin\alpha}P_{k0}R\sin\varphi\left(e^{-Bt/\sqrt{2}} - e^{-\sqrt{2}Bt}\right)$
	$\varphi = \frac{\pi}{2} - \alpha \sim \pi$	$Q_{pk\varphi} = \left(e^{-Bt/\sqrt{2}} - e^{-\sqrt{2}Bt}\right)\left[\frac{(1 - \cos 2\alpha)}{4\sin\alpha}P_{k0}R\sin\varphi - \frac{1}{2}P_{k0}R\left(1 - \frac{\cos\varphi}{\sin\alpha}\right)(\sin\alpha - \cos\varphi)\sin\varphi\right]$
Opposite force distribution of triangle	$\varphi = 0 \sim \frac{\pi}{2}$	$Q_{K\varphi} = \frac{1}{4\pi}\frac{D^3}{2r^3}\left(e^{-Bt/\sqrt{2}} - e^{-\sqrt{2}Bt}\right)F_{\max}\sin\varphi$
	$\varphi = \frac{\pi}{2} \sim \pi$	$Q_{K\varphi} = \frac{D^3}{2r^3}\left(e^{-Bt/\sqrt{2}} - e^{-\sqrt{2}Bt}\right)F_{\max}\left(\frac{1}{4\pi}\sin\varphi - \cos^3\varphi\right)$
Opposite force distribution of uniform	$\varphi = 0 \sim \frac{\pi}{2}$	$Q_{K\varphi} = 0.053\frac{D^3}{2r^3}\left(e^{-Bt/\sqrt{2}} - e^{-\sqrt{2}Bt}\right)F_{\max}\sin\varphi$
	$\varphi = \frac{\pi}{2} \sim \pi$	$Q_{K\varphi} = \frac{D^3}{2r^3}\left(e^{-Bt/\sqrt{2}} - e^{-\sqrt{2}Bt}\right)F_{\max}\left(0.5\sin\varphi\cos\varphi - 0.5\cos\varphi + 0.053\sin\varphi\right)$

Appendix

See Tables 15, 16, and 17.

Competing Interests

The authors declare that there are no competing interests regarding the publication of this article.

Acknowledgments

This work is supported by the National Natural Science Foundation of China (no. 51378051 and no. 51678038), the Fok Ying Tung Education Foundation (no. 122009), and the Fundamental Research Funds for the Central Universities (no. 2011JBZ008).

References

[1] W. Sun, *The Comparison of Internal Force Formula on the Condition of Different Partial Load Forms Based on FFD*, Beijing Jiaotong Unveirsity, Beijing, China, 2014.

[2] L. Fernandez-Moguel and J. Birchley, "Analysis of the accident in the Fukushima Daiichi nuclear power station unit 3 with MELCOR_2.1," *Annals of Nuclear Energy*, vol. 83, no. 9, pp. 193–215, 2015.

[3] J. W. Park and W.-C. Seol, "Considerations for severe accident management under extended station blackout conditions in nuclear power plants," *Progress in Nuclear Energy*, vol. 88, no. 4, pp. 245–256, 2016.

[4] L. M. Bresciani, A. Manes, T. A. Romano, P. Iavarone, and M. Giglio, "Numerical modelling to reproduce fragmentation of a tungsten heavy alloy projectile impacting a ceramic tile: adaptive solid mesh to the SPH technique and the cohesive law," *International Journal of Impact Engineering*, vol. 87, no. 1, pp. 3–13, 2016.

[5] M. Pastor, B. Haddad, G. Sorbino, S. Cuomo, and V. Drempetic, "A depth-integrated, coupled SPH model for flow-like landslides and related phenomena," *International Journal for Numerical and Analytical Methods in Geomechanics*, vol. 33, no. 2, pp. 143–172, 2009.

[6] M. G. A. Huigen, "First principles of the MameLuke multi-actor modelling framework for land use change, illustrated with a Philippine case study," *Journal of Environmental Management*, vol. 72, no. 1-2, pp. 5–21, 2004.

[7] J. Liu and X. Hou, *Shield Tunnel*, China Railway Press, Beijing, China, 1991.

[8] X.-H. Li, Y. Long, C. Ji, X. Zhou, Y.-Y. He, and L. Lu, "Analysis of dynamic stress concentration factor for existing circular tunnel lining under blasting seismic wave," *Rock and Soil Mechanics*, vol. 34, no. 8, pp. 2218–2223, 2013.

[9] M. Liqiu, *The Dynamic Centrifugal Model Test and Numerical Study of the Shallow Buried Tunnel under Blast Loading*, Tsinghua University, 2010.

[10] Y. Wang, L. Kong, A. Guo et al., "Model test research on influences of shallow gas stratum on stability of metro tunnel," *Rock and Soil Mechanics*, vol. 31, no. 11, pp. 3425–3428, 2010.